processes

MDPI

Article

Optimized Layout for High-Level Drilling in a High-Gas Coal Seam to Prevent Gas Overrun

Kun Gao [1,2] and Shuonan Ma [1,2,*]

[1] College of Safety Science and Engineering, Liaoning Technical University, Huludao 125100, China; lnfsgk@163.com
[2] Key Laboratory of Mine Thermal Power Disaster and Prevention and Control of Ministry of Education, Liaoning Technical University, Huludao 125100, China
* Correspondence: shuonanma@gmail.com

Abstract: With the popularization of comprehensive mechanized mining methods and the increase in coal mining intensity, production has become more concentrated and efficient, which inevitably leads to Coal seam accumulates a large amount of gas The existence of huge goaf and mining overburden cracks that form behind the working face provides favorable conditions for the migration of gas to the goaf and its subsequent accumulation. The high concentration of gas that accumulates in the goaf gradually flows toward the working face under the action of pressure and concentration gradients, which can easily cause gas overrun accidents at the working face. Therefore, effective relief of the gas pressure in the goaf is important to guarantee safe and efficient mining at the coal mine working face. One of the most used gas drainage methods in such mines is high-level borehole gas drainage. This method can effectively reduce the gas content of coal seams, ensure the safe production of working faces, and reduce carbon emissions. In this study, the mining of a high-gas and low-permeability extra-thick coal seam in the Shanxi mining area is taken as the engineering background. In order to optimize the extraction design and improve the efficiency of gas extraction, according to the dual characteristics of coal seam pores and cracks, the permeability, and migration form of the gas in the coal body are analyzed, and a COMSOL coal seam gas migration model is established. By controlling different gas extraction horizons, pressure, and the number of boreholes and by optimizing the trajectory of the boreholes, the law of gas migration during high-level borehole gas extraction and the variation law with extraction time and pressure are studied. From this, the effective extraction calculation formula is fitted and statistical analyses are carried out. Through on-site extraction and simulation verification, the gas concentration was found to reach a maximum of 86% at a distance of 23 m from the floor. When using similar extraction times, 20 MPa gas extraction was found to have the best effect. The highest gas concentration in the upper corner was only 0.71%, and the extraction efficiency is higher when the high-level borehole trajectory angle is 30 degrees. The research results have important reference value for gas disaster control in the fully mechanized caving face of high-gas low-permeability and extra-thick coal seams.

Keywords: gas extraction; extra-thick coal seam; gas migration; high gas; low permeability

check for updates

Academic Editor: Carlos Sierra Fernández

Received: 23 December 2024
Revised: 23 February 2025
Accepted: 25 February 2025
Published: 27 February 2025

Citation: Gao, K.; Ma, S. Optimized Layout for High-Level Drilling in a High-Gas Coal Seam to Prevent Gas Overrun. *Processes* **2025**, *13*, 688. https://doi.org/10.3390/pr13030688

Copyright: © 2025 by the authors. Licensee MDPI, Basel, Switzerland. This article is an open access article distributed under the terms and conditions of the Creative Commons Attribution (CC BY) license (https://creativecommons.org/licenses/by/4.0/).

1. Introduction

Coal mining is always accompanied by many disasters and accidents [1], mainly manifesting as rock bursts, the frequency of which increases as gas pressure and content increase with mining depth. Furthermore, the number of gas-related disasters is increasing [2]. Due

to the recommendations from the 18th National Congress of the Communist Party of China, China has gradually implemented a national policy for reducing the production capacity of small coal mines, and shutting them down or integrating them into larger mines; coal production has thus been greatly limited. However, China is still a major global producer and consumer of coal. In 2015, coal production by enterprises was about 8 billion tons, and China's production reached 3.75 billion tons [3]. Even though there has been a 3.3% year-on-year reduction in coal production, China's output represents 47% of the global total. In addition, China's coal consumption was 3.965 billion tons [4], a year-on-year decrease of 3.7%; however, this still accounted for a large proportion of global coal consumption.

The number of accidents in China's coal mines is quite large, mainly manifesting as coal and gas outbursts [5], coal mine gas explosions, gas combustion and room-breathing issues, roof collapses, and rock bursts [6]. Accidents caused by gas are quite serious; these types of accidents not only cause a large number of casualties but also may cause the long-term shutdown of coal mines and lead to large economic losses. When gas accumulates to a certain volume fraction, different phenomena will occur. When the volume fraction is greater than 15%, it may cause gas combustion accidents; when the volume fraction reaches 5~15%, it may cause gas explosion accidents [7]. Excessive gas accumulation will also reduce the concentration of oxygen in the air, resulting in difficulty breathing, which may cause room-breathing issues. A coal and gas outburst is the unstable release of the stress energy and gas energy stored in coal. The sudden release of coal seam gas energy poses a major threat to the personal safety of the working-face personnel, wastes a significant amount of gas resources, and pollutes the environment. The greenhouse gas effect of methane, the main component of this gas [8], is more than 20 times larger than that of CO_2.

Therefore, coal seam gas extraction has important significance and a far-reaching impact on coal mines: it can reduce environmental pollution and improve the strength of coal, reduce the gas energy stored in the coal seam, and prevent coal and gas outbursts. Moreover, an increase in the clean energy utilization of methane saves on coal resources and achieves circular development, and a reduction in gas accumulation creates a good ventilation environment. To prevent gas overrun, we need to create favorable conditions for mine ventilation [9].

Gas extraction involves drilling holes or roadways in areas with high gas concentrations. By setting the extraction nozzle to a negative pressure, a pressure difference forms between the nozzle and the surrounding air pressure, and the gas flows from areas of high pressure toward the extraction pipeline [10] and then through the pipeline connected to the nozzle; the gas is then continuously transported to a ground gas reservoir. Thus, the gas concentration of the coal seam can be effectively controlled, and the probability of gas explosions will be greatly reduced [11]. At the same time, moving gas from high-concentration areas toward the ground serves a secondary purpose. Gas combustion can release high amounts of heat. During daily life [12], this heat-generating capacity can be utilized to cook food and heat homes via the use of natural gas and can be used in the form of liquefied petroleum gas for industrial production. Therefore, the number of gas uses is very extensive. To solve the problem of gas accumulation, most mines in China have adopted high-drainage roadways and special gas-drainage roadways to extract gas [13]. Among them, the use of special gas-drainage roadways to effectively extract high-concentration gas is difficult, with the extraction effect not ideal and certain safety hazards present. Therefore, new regulations have been set such that mines can no longer continue to use special gas-drainage roadways to extract gas [14]. However, high-drainage roadways also have some problems, such as their long construction time, alternating tension between mining and excavation, high construction costs, and so on [15]. Due to these limitations, the method of high-level borehole gas extraction emerged [16]. Owing to its controllable drilling trajectory, long

drilling distances, large-scale gas extraction, and significant extraction effect, high-level directional drilling is increasingly used in high-level fracture gas extraction in coal mines. The coal seam gas content of the 81201 coal mining face in a coal mine in Shanxi is high, and the gas emission in the goaf is large [17], which leads to high gas concentrations in the return-air lane and the return-air corner [18]. In order to effectively manage the gas in the goaf, this study analyzes the gas extraction principle and the advantages of high-level directional long boreholes; optimizes the gas extraction horizon, pressure, and borehole trajectory parameters; and finally achieves good results [19].

General Situation of the Working Face

The 81201 working face is situated in the southern region of the primary and auxiliary roadways within the third panel, north of the mine field boundary, east of the 81308 working face goaf, and west of the 81202 working face. The elevation of the working face ranges from 908 to 1134 m, with the floor elevation spanning from 607.5 to 650.1 m. The average thickness of the coal seam at the 81201 fully mechanized top coal caving face is 7.0 m, and the dip angle varies between 3 and 6 degrees. The working face is configured to follow the seam's trend and progresses along the strike [20]. The face's advancement is 2575 m in length, with a width of 240 m. The mine was designed to have a height of 3.7 m, a caving height of 3.3 m, and a mining-to-caving ratio of 1:0.89. In this study, the longwall-retreating comprehensive mechanized caving coal mining method was employed. The occurrence of coal seam characteristics for all caving working faces is detailed in Table 1. Additionally, the roof and floor characteristics of the coal seam at the working face are outlined in Table 2.

Table 1. Characteristics of coal seam occurrence.

Average Thickness (m)	7.0	Coal Seam Structure	1.6(0.1)1.6(0.4)1.3(0.5)1.5	Coal Seam Dip Angle	3~6°
Coal seam situation	The coal seam structure is complex, and the macroscopic coal rock type is mainly semi-bright–semi-dark coal. The average thickness of the coal seam is 7.0 m (5.8 m–8.6 m), the average coal seam comprises three layers, and the maximum thickness of the local single layer is 1.6 m, which is located near the five joint roadways of the working face. The expected coal seam structure is 1.6 (0.1) 1.6 (0.4) 1.3 (0.5) 1.5; a layer of thick parting is present in the 8-2 coal of the mining section, with a thickness of about 0.5 m; the coal is gas coal. The coal seam is generally thicker in the withdrawal channel and the open-off cut and thinner in the middle. The recoverable index of the coal seam is 1, and the coefficient of variation is 27.5%, making it a relatively stable coal seam.				

Table 2. Characteristics of the top and bottom plates of the coal seam.

Top, Bottom	Rock Stratum Name	Thickness Range (m)	Lithological Characteristics
Old roof	Coarse-grained sandstone, gravel coarse sandstone	4.5–10.1	It is grayish white, mainly composed of quartz, followed by feldspar, containing dark debris.
Immediate roof	Mudstone, medium-grained sandstone	0.3–2.0	Sandy mud structure, horizontal texture, flat structure, containing a small amount of incomplete plant fossils.
Direct bottom	Mudstone, sandy mudstone, siltstone	0.62–2.6	Deep gray mudstone, medium grained, siltstone, thin-layer structure.

The mine is classified as a high-gas mine. Based on the outcomes of gas grade identification conducted between 2021 and 2022, the mine's absolute gas emission stands at 119.59 cubic meters per minute, with a relative gas emission of 10.72 cubic meters per ton. Consequently, it is categorized as a high-gas mine.

The extractability of coal gas is primarily influenced by the permeability coefficient of the coal seam and the attenuation coefficient of borehole flow. It is also affected by the gas pressure within the coal seam and the gas emission rate at the working face. An analysis of the measured data reveals that the permeability coefficient of the 81201 working face in the No. 8 coal seam is 0.884, while the gas pressure exceeds 0.74 MPa, indicating a potential risk of outburst. Moreover, the gas emission rate at the working face is 5.44 m^3/t, and the attenuation coefficient for borehole gas flow is 0.016 d^{-1}. According to the established criteria for classifying extraction difficulty [21], a coal seam is considered extractable when the attenuation coefficient of borehole gas flow ranges from 0.003 to 0.05 and the permeability coefficient of the coal seam falls between 0.1 and 10. Consequently, the coal seam gas at the 81201 working face meets these criteria, qualifying it as a seam suitable for gas extraction [22].

2. Establishing a Goaf Model

2.1. Establishing the Basic Data

Based on the general conditions of the work area and the roadway layout detailed in the foundational data, we streamlined the model dimensions for the 81201 work area. The model was constructed as follows:

(1) The caving and fracture zones of the 81201 coal mining face, the main and auxiliary air intake roadways, and the goaf are represented using simplified cuboid three-dimensional graphics. This representation does not take into account the presence of electrical equipment, transportation belts, gas extraction pipelines, wind and water pipelines, or personnel on the roadways [23].

(2) Based on the calculations derived from mathematical formulas and the analytical outcomes of the 3dec simulation software, using our model, we established the collapse height of the compaction zone within the goaf at 17 m. Above the roof, the gas transport channel is designated as the fracture zone, which has a height of 38 m. Given the minimal amount of gas desorption and storage above the fracture zone, our model does not specifically address the bending and sinking of the upper rock strata.

(3) The size of the goaf is set to 300 m (strike) × 240 m (tendency) × 55 m (roof direction). The caving zone is set to different sizes due to the large morphological changes: 0 m to 30 m, 30 m to 150 m, and 150 m to 300 m [23].

(4) The size of the roadway is 40 m × 4 m × 8 m, the size of the working face is 240 m × 4 m × 8 m, the size of the caving zone is 300 m × 240 m × 17 m, and the size of the fracture zone is 300 m × 240 m × 38 m.

The model established using the COMSOL simulation software (COMSOL Multiphysics 6.2) according to these model parameters is shown in Figure 1.

The gas within the goaf predominantly consists of a blend of methane and air. In the model, the intrinsic properties of the gas are not taken into account, and the impacts of temperature, humidity, and other unmanageable variables are disregarded. By employing this simplification [24], the investigation of the gas flow dynamics and extraction efficacy within the goaf becomes more focused, thereby offering a robust theoretical foundation for gas management. The physical model and mesh dimensions of the goaf are depicted in Table 3.

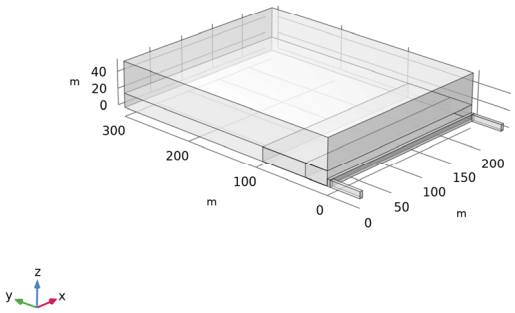


Figure 1. The goaf model.

Table 3. Dimensions of the physical model of the mining area.

Name	Dimension/m	Mesh Subdivision/m
Fracture zone	300×240×38	2
Natural accumulation area	30×240×25	1
Load-affected zone	120×240×25	2
Stable compaction zone	240×240×25	2
Working surface	8×240×4	1
Auxiliary air intake roadway	40×4×8	1
Return laneway	40×4×8	1

We integrated the constructed model into our software to execute grid segmentation tasks, as depicted in Figure 2. Selecting the optimal mesh type and size is crucial for the precision of subsequent simulation outcomes [25]. Given that our modeling subject possesses a regular shape, we established a grid scale of 2 m for the bearing capacity zone, the stable filling zone, and the crack zone. Conversely, for the working surface, the sections transitioning into or out of the tunnel, and the natural accumulation zone, a grid scale of 1 m was implemented. Based on the simulation outcomes, we can delineate the model using a structured grid, resulting in a total of 1,436,782 Network cell with an average grid quality of 0.98. Extensive simulation testing revealed that when the average grid quality surpasses 0.95, its influence on the simulation results is relatively minor [26].

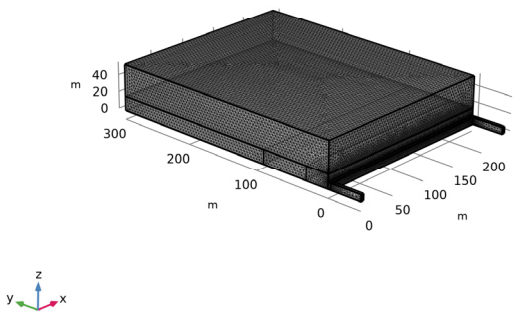


Figure 2. Grid division diagram.

2.2. Goaf-Related Parameter Setting

(1) Calculation of porosity, permeability, viscous resistance, and inertial resistance

Porosity refers to the ratio of the total volume of pores in the porous medium to the volume of the porous medium. The more internal pores in the coal, the easier it is for gas to migrate in coal. According to this definition, the formula for porosity can be obtained [27]:

$$n = \frac{v_k}{v} \times 100\% \quad (1)$$

In this formula, n is porosity; v_k is the total volume of the pores, in m^3; and v is the volume of porous media, in m^3.

According to the definition of the broken expansion coefficient, the larger the broken expansion coefficient, the larger the small coal and rock mass after caving and crushing, and the more broken coal. The more pores within the rock masses, the greater the porosity, so a certain conversion relationship exists between the expansion coefficient and porosity [28].

Porosity n is calculated using the following formula:

$$n = 1 - \frac{1}{k_p} \quad (2)$$

In this formula, k_p is the expansion coefficient of coal and rock mass.

Permeability a is calculated using the following formula:

$$a = \frac{D^2_p}{150} \frac{n^2}{(1-n)^2} \quad (3)$$

Among the number of constantly changing, particle size D_p of the compressed body in the goaf is calculated using the following formula:

$$D_P = \left\{ \begin{array}{l} 5 \times 10^{-5}x^2 - 1 \times 10^{-3}x + 0.1 (x \leq 100) \\ 0.05 (x > 100) \end{array} \right\} \quad (4)$$

In this formula, D_P is the particle size of a compressed body in the goaf, in m, and x is the distance between the goaf and the working face, in m.

The product of the viscous resistance coefficient R_f and permeability a in the goaf is 1, so the expression for calculating R_f is as follows:

$$R_f = \frac{1}{a} = \frac{150(1-n)^2}{D^2_p n^2} \quad (5)$$

The inertial resistance is calculated using the following formula [29]:

$$P_f = \frac{3.5(1-n)}{D_p n^3} \quad (6)$$

According to the calculation of the above formula, the parameters needed for gas extraction in the goaf are obtained. The data are shown in Table 4.

Porosity, permeability, and the expansion coefficient affect the measurement results due to the changes in measurement methods, experimental conditions, fluid properties, and experimental equipment accuracy, which result in errors. The specific error should be controlled in the numerical ranges reported in Table 4.

Table 4. Model parameter settings.

Name	Porosity	Permeability/K	Bulking Coefficient/m^2
Fracture zone	0.029 ± 0.002	$(2.64 \pm 0.04) \times 10^{-8}$	1.05 ± 0.02
Natural accumulation area	0.333 ± 0.010	$(9.91 \pm 0.02) \times 10^{-6}$	1.40 ± 0.12
Load-affected zone	0.167 ± 0.001	$(1.87 \pm 0.01) \times 10^{-6}$	1.22 ± 0.04
Compaction stable area	0.091 ± 0.012	$(1.97 \pm 0.02) \times 10^{-7}$	1.10 ± 0.05

(2) Determination of the gas quality source term

The gas from the 81201 working face of the coal mine in Shanxi is emitted at 21 m^3/min, that from the goaf is 12.2 $m^{3/}$min, that from the caving zone is 3.2 m^3/min, and that from the fractured zone is 9.1 $m^{3/}$min, calculated according to the following formula:

$$Q_s = \frac{Q_a \cdot \rho_{cH4}}{V_a} \tag{7}$$

In this formula,

Q_s is the gas quality source term, in kg/(m^2·s);
Q_a is the gas emission quantity, in m^3/s;
ρ_{cH4} is the gas density, in kg/m^3, 0.717 kg/m^3;
V_a is the gas emission volume, in m^3.

① Gas quality source term of the working face:

$$\frac{\frac{21}{60} \times 1000 \times 0.717}{(240 \times 4 \times 8) \times 22.4} = 1.46 \times 10^{-3} \cdot \text{mol}/(\text{m}^3 \cdot \text{s})$$

② Gas quality source term of the fracture zone:

$$\frac{\frac{9.1}{60} \times 1000 \times 0.717}{(240 \times 300 \times 38) \times 22.4} = 1.77 \times 10^{-6} \cdot \text{mol}/(\text{m}^3 \cdot \text{s})$$

③ Gas quality source term of the caving zone:

$$\frac{\frac{3.2}{60} \times 1000 \times 0.717}{(240 \times 300 \times 17) \times 22.4} = 1.39 \times 10^{-6} \cdot \text{mol}/(\text{m}^3 \cdot \text{s})$$

Within the goaf, we determined the gas quality source term for each region based on the broken expansion coefficient and computed the average broken expansion coefficient for the caving zone using the provided formula.

$$\frac{1.4 \times 30 + 1.22 \times 60 + 1.1 \times 210}{30 + 60 + 210} = 1.154$$

① Gas quality source term in a natural accumulation area:

$$\frac{1.4}{1.15} \times \frac{30}{300} \times 2.51 \times 10^{-6} = 3.06 \times 10^{-7}\ \text{kg}/(\text{m}^3 \cdot \text{s})$$

② Gas quality source term in a load-affected zone:

$$\frac{1.22}{1.15} \times \frac{60}{300} \times 2.51 \times 10^{-6} = 5.33 \times 10^{-7}\ \text{kg}/(\text{m}^3 \cdot \text{s})$$

③ Gas quality source term in a stable compaction area:

$$\frac{1.1}{1.15} \times \frac{210}{300} \times 2.51 \times 10^{-6} = 1.68 \times 10^{-6}\ \mathrm{kg/(m^3 \cdot s)}$$

Utilizing the calculation formula for the aforementioned gas quality source term, the parameters for each zone within the goaf have been determined, as illustrated in Table 5. Subsequently, the boundary conditions have been established based on the aforementioned data [30].

Table 5. Gas source item setting parameters.

Area	Working Surface	Fracture Zone	Natural Accumulation Area	Load-Affected Zone	Stable Compaction Zone
Gas source term kg/(m^{3}s)	$(1.46 \pm 0.02) \times 10^{-3}$	$(1.77 \pm 0.03) \times 10^{-6}$	$(3.06 \pm 0.02) \times 10^{-7}$	$(5.33 \pm 0.04) \times 10^{-7}$	$(1.68 \pm 0.02) \times 10^{-6}$

Due to complex geological conditions, the uneven spatial distribution of parameters such as coal seam permeability and porosity leads to inaccurate estimations of gas source terms. The error determined through formula calculation, which has little effect on the value, is about 0.02.

3. Optimizing the Spatial Horizon of High-Level Boreholes

Based on mining fracture theory for an 'O'-type circle and the analysis of its evolving patterns, this study examines the spatial distribution factors of high-level boreholes to subsequently identify the optimal elevation for gas extraction [31].

3.1. Gas Distribution in the Goaf

The law of gas migration and distribution in the goaf is intuitively reflected by the gas distribution when gas is not extracted (Figure 3).

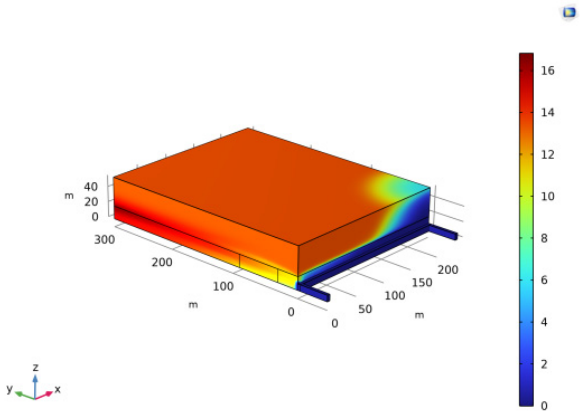
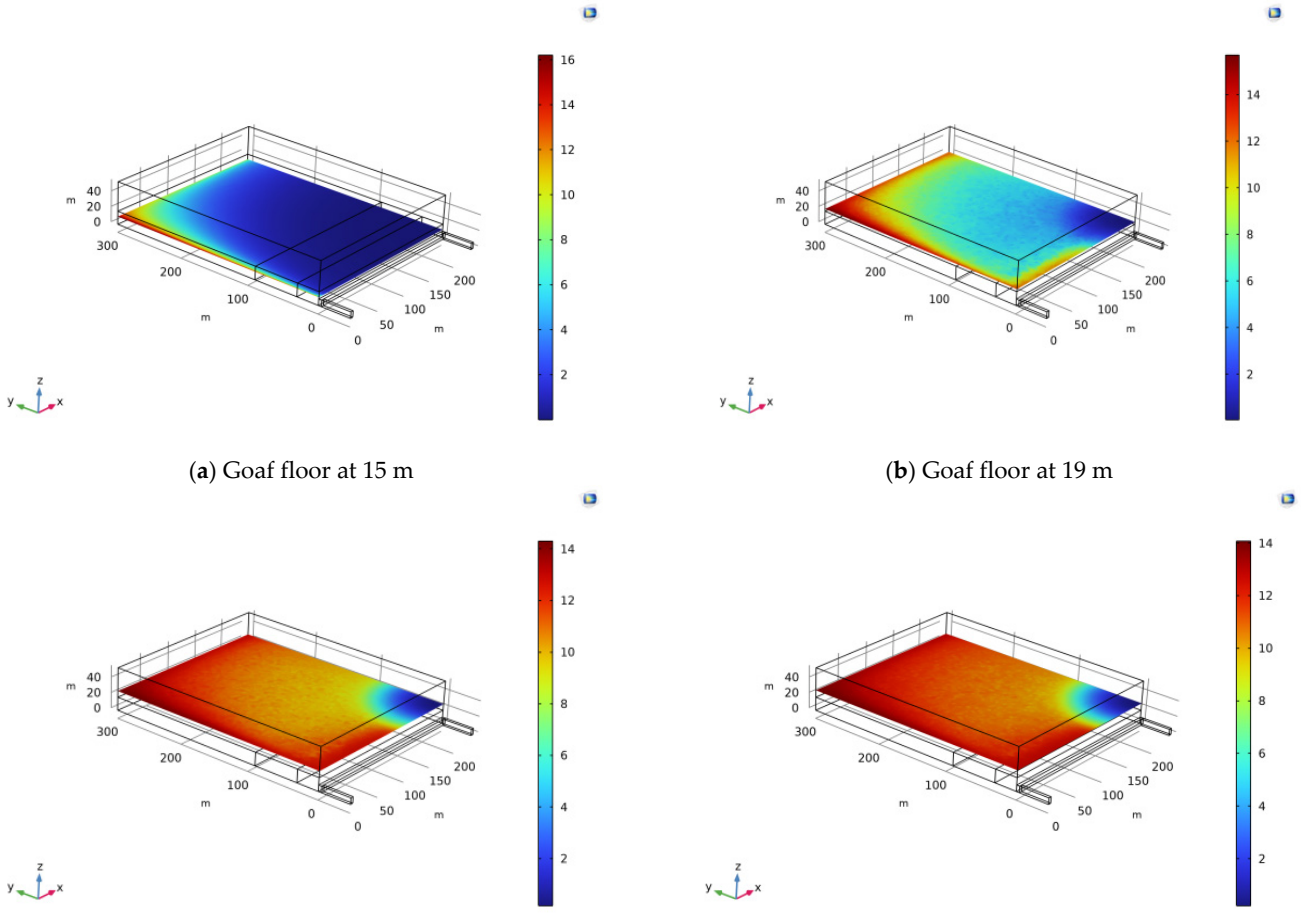


Figure 3. A 3D distribution diagram of the gas concentration in the goaf area.

In the absence of additional interventions, the dispersion of gas concentrations via the ventilation system reveals that air currents traverse the main shaft and extend into the work zone. Certain gasses are propelled by the pressure of the airflow and exit through the rear shaft, while other air currents, influenced by negative pressure, transport gasses deeper into the mining cavity. Typically, the mining space adjacent to the work area does not readily experience gas accumulation, as there is an abundance of falling gravel, creating a network of pores and fissures [32].

3.2. Gas Migration Under Different Floor Heights

According to the control variable method, the gas migration law is observed for floors with heights of 15 m, 19 m, 23 m, and 26 m in the goaf (Figure 4).



(**a**) Goaf floor at 15 m

(**b**) Goaf floor at 19 m

(**c**) Goaf floor at 23 m

(**d**) Goaf floor at 26 m

Figure 4. (**a**–**d**) Gas distribution in the different layers.

When Z equals 15 m, all airflow within the working face is expelled via the return airway, leading to a significant buildup of gas on the return side of the working face [16]. Influenced by mining activities, a series of alterations transpire in the upper region of the working face: these include the creation of a caving zone and a fracture zone, which progressively deteriorate the rock structure above and induce various vertical or transverse fissures. Among them, the section below 17 m is the caving zone, and the air flow dynamics under it can discharge some of the gas in the goaf to the external environment. Similarly, Z = 19 m, Z = 23 m, and Z = 26 m are located in the fracture zone. Because the density of gas is less than that of air, when the pressure increases, density increases and the gas tries to disperse into other spaces, thus slowly penetrating into the fracture zone. At the same time, because the gas in the roof is compressed during mining, the solubility of the gas in the roof increases, which causes gas to accumulate in the roof, and finally reaches a stable distribution state [33].

3.3. Z Axis ⊥ XY Plane Profile

Regarding the tendency of the goaf, cross-section maps are established at positions 20 m, 40 m, 60 m, 80 m, and 100 m from the main air intake roadway, as shown in Figure 5.

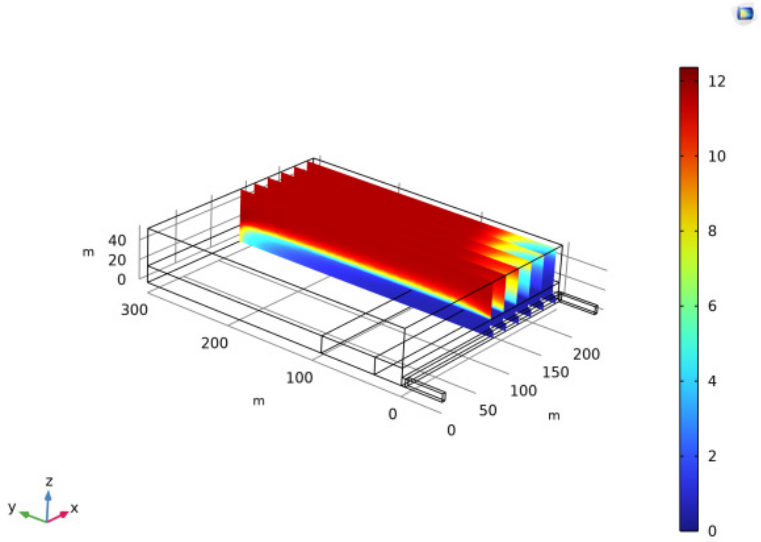


Figure 5. An inclined gas distribution diagram of the goaf.

Along the inclination of the working face, the airflow enters the working face from the air inlet roadway, thus removing any harmful gasses and providing oxygen to the staff, and the gas concentration in the upper corner is large.

3.4. Plane Profile Along the X Axis

In the direction of the goaf, cross-sections are established at 50 m, 90 m, 130 m, 170 m, etc., from the working face, as shown in Figure 6.

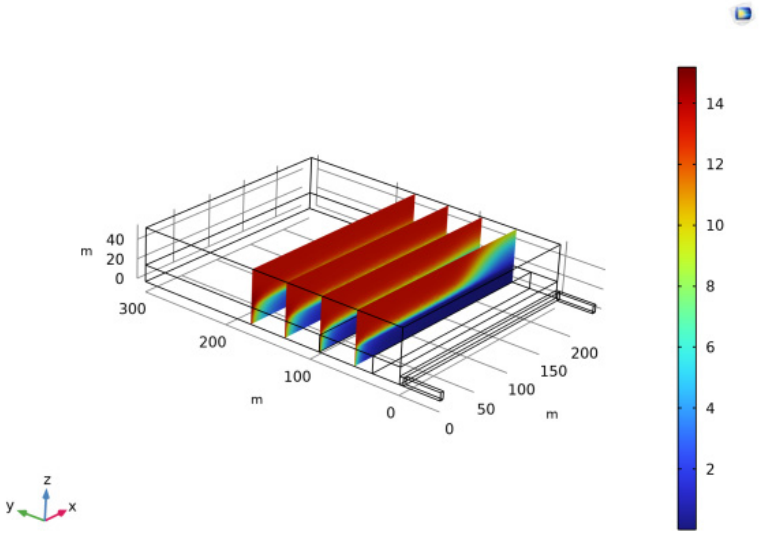


Figure 6. Gas distribution diagram of the goaf direction.

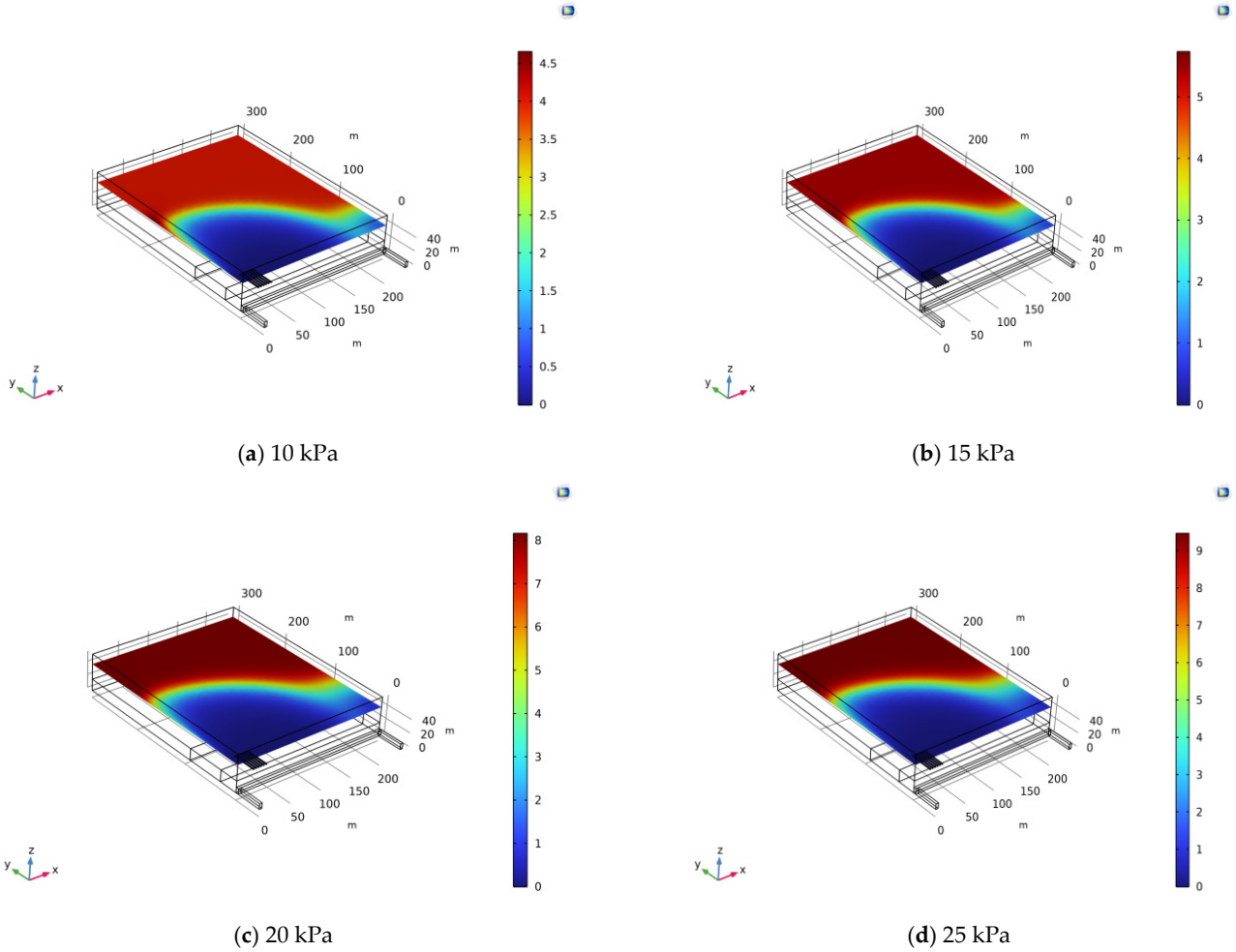
In the vicinity of the goaf area along the X-axis, numerous rocks have recently detached from the working surface, resulting in a state of unconfined accumulation, characterized by substantial porosity. As air infiltrates the mined-out region, gas permeates to greater depths, with porosity diminishing as depth increases. Upon reaching a critical porosity threshold, the overlying strata collapse and become essentially compacted. From this perspective, the trend for gas concentration is observed to increase from shallow to deep zones.

3.5. The Influence of Extraction Negative Pressure on Extraction Effect

The horizontal distance X from the high-level borehole to the return airway is calculated according to the following formula:

$$\frac{\mathrm{H}}{\tan(\theta+\delta)} \leq X \leq \frac{L}{3} \tag{8}$$

X is between 9.8 m and 31 m, with drilling intervals of 4 m between six holes. Based on these initial conditions, an extraction model is established. When the vertical height is 23 m, a simulation experiment control group with different pressure values is set up using COMSOL, as shown in Figure 7a–d.



(**a**) 10 kPa (**b**) 15 kPa

(**c**) 20 kPa (**d**) 25 kPa

Figure 7. (**a**–**d**) Different extraction negative pressure gas concentration distribution.

The diagram above illustrates the distribution of gas concentration within the goaf under varying levels of negative pressure during drainage. In contrast to the conditions prior to implementing the extraction measures, the gas concentration in the goaf significantly decreases as the drilling extraction pressure increases. The influence of high-level boreholes becomes apparent; as the extraction pressure rises from 10 kPa to 20 kPa, a substantial amount of high-concentration gas that accumulated at the top of the goaf is efficiently removed. Concurrently, the gas within the central region of the goaf, subjected to the effects of the extraction, begins to migrate towards the high-level boreholes, thereby markedly enhancing the extraction efficiency of gas from the goaf. When the extraction pressure is further elevated to 25 kPa, the rate of gas extraction decreases and stabilizes [34].

Upon evaluating the extraction scheme, we find that setting the extraction negative pressure at 20 kPa results in a relatively safe gas concentration in the upper corner, and the borehole extraction performance is commendable. The experimental data suggest that the optimal extraction pressure should be established at 20 kPa. Through various simulation strategies, we deduce that the optimal drilling position should be approximately 23 m above the coal surface. Under these specific conditions, the range of gas concentrations accessible via our suction holes is between 3% and 18%, while the gas content at the corner varies from 0.35% to 0.46%, indicating favorable gas extraction efficiency.

4. Gas Extraction Trajectory Optimization

4.1. Comparison of Two Extraction Methods

The conventional extraction technique is depicted in Figure 8. As the fracture zone naturally collapses following coal seam extraction, the No. 1 borehole becomes obstructed by rocks, preventing it from accessing the fracture zone. Consequently, the gas within the fracture zone remains unextracted. Therefore, it becomes essential to redrill a new borehole, No. 2, which demands significant labor and material resources, and the extraction results are often suboptimal.

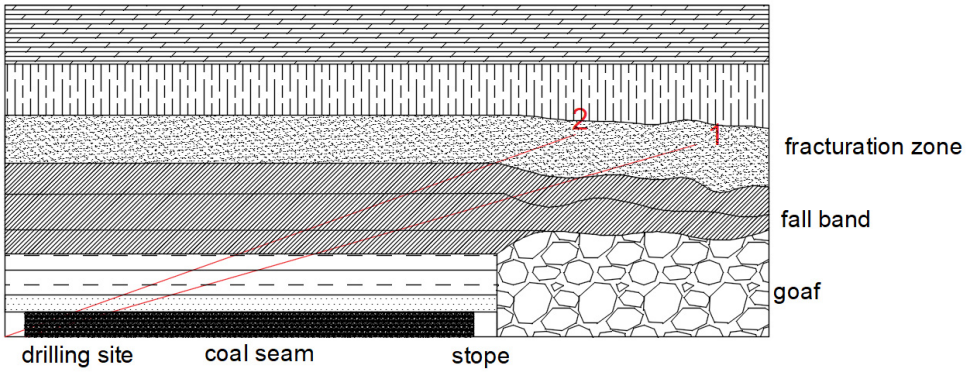


Figure 8. Gas extraction trajectory.

As shown in Figure 9, the optimized drilling trajectory avoids the problem of the borehole being blocked due to a collapse in the fracture zone and a new borehole needing to be drilled. The optimized drilling trajectory has a good extraction effect and a long extraction time; this trajectory can be used for a long time and saves on costs.

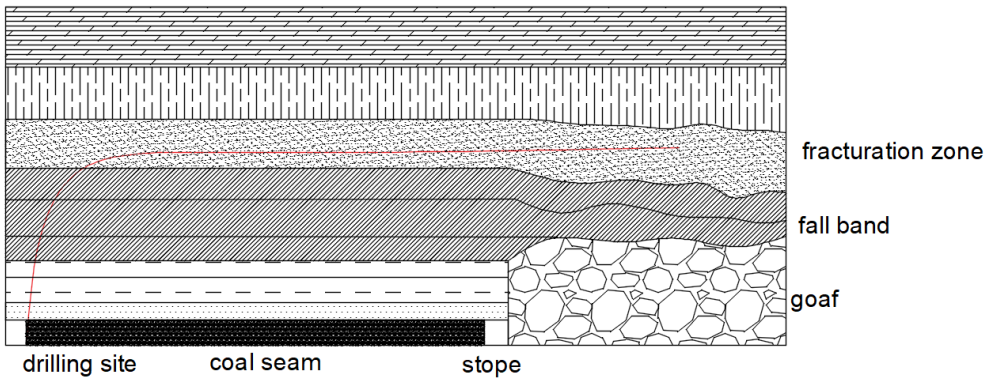
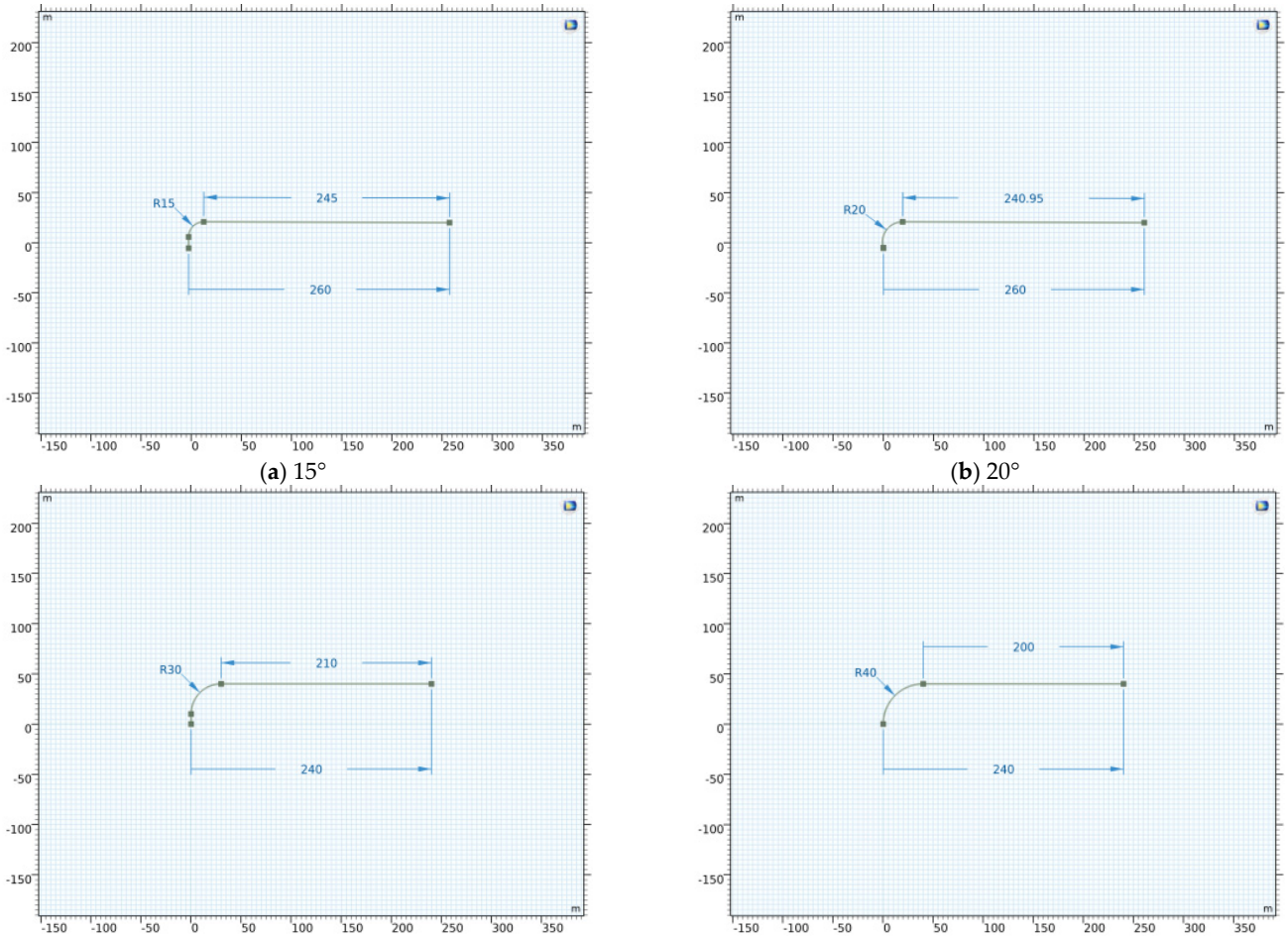


Figure 9. Optimized gas extraction trajectory.

4.2. Drilling Parameter Arrangement

The gas extraction pipeline model was established in COMSOL software (COMSOL Multiphysics 6.2) to set the following parameters to measure the gas flow rate.

The model was constructed using COMSOL software, with directional long borehole trajectories created at rotation angles of 15°, 20°, 30°, and 40°. The overall length of the borehole trajectory measured 240–260 m. Following two reaming processes, the diameter of the hole reached 115 mm, the extraction negative pressure was set at 20 kPa, and the drilling height was set at 23 m as it was the best extraction layer (Figure 10).



(**a**) 15° (**b**) 20°

(**c**) 30° (**d**) 40°

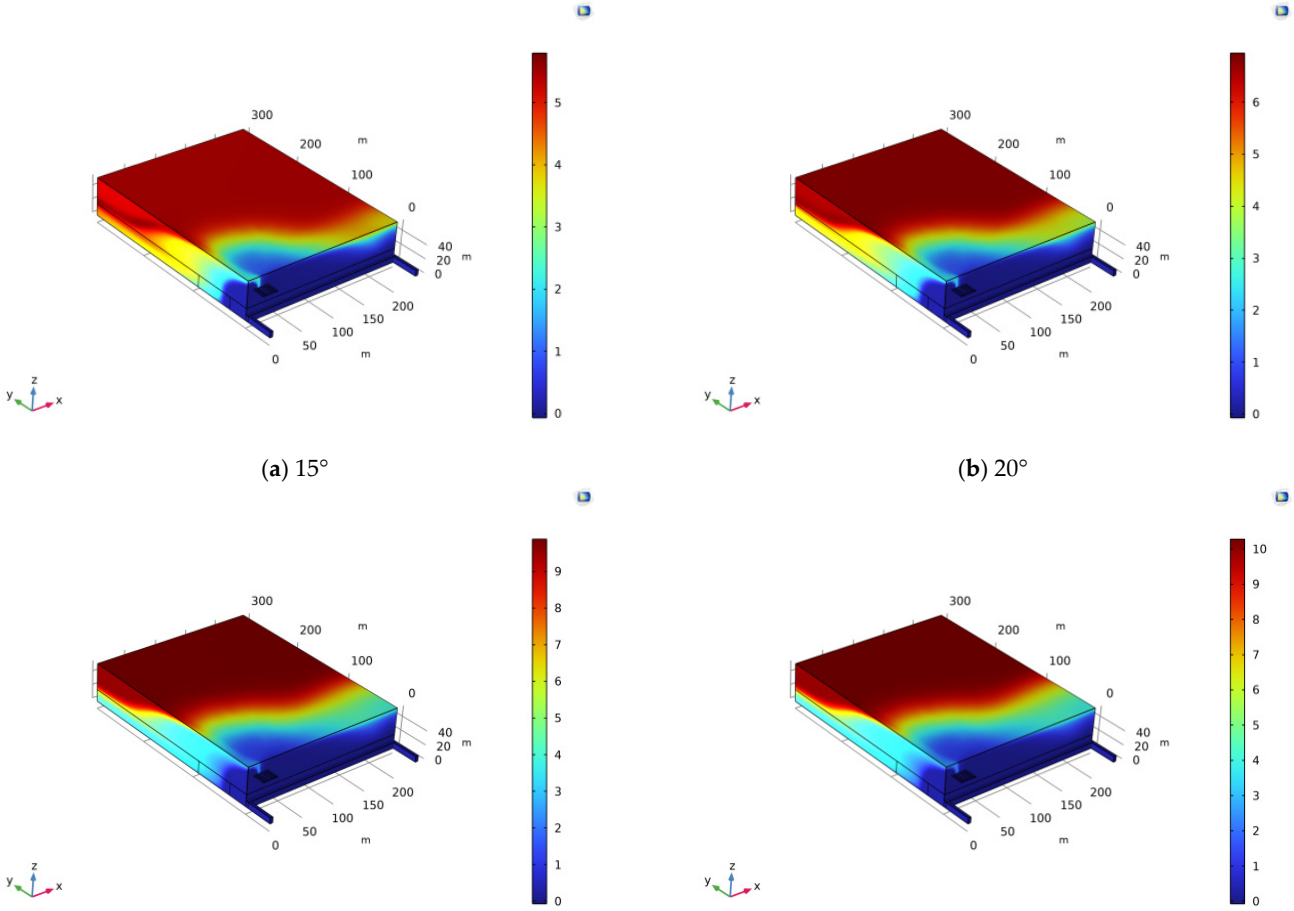
Figure 10. (**a**–**d**) Extraction trajectory parameter diagram.

4.3. Numerical Simulation Results and Analysis of Gas Extraction Effect

Taking an extraction duration of 20 days as an example, the following simulation diagram was obtained via numerical simulation [35].

Figure 11a,b are the gas distribution concentration maps for 20 days when the gas extraction trajectory angles are 15° and 20°. Red represents a high gas concentration, and blue represents a low gas concentration.

As illustrated in the figure above, the volume of extracted gas experiences a rapid increase as the number of rotation angles shifts from 15° to 20°. Subsequently, when the angle increases from 20° to 30°, the gas drainage volume rises at a slower pace. Between 30° and 40°, the amount of extracted gas remains essentially constant, indicating that the optimal angle for extraction is at 30°.



(**a**) 15° (**b**) 20°

(**c**) 30° (**d**) 40°

Figure 11. (**a**–**d**) Gas extraction concentration diagram.

5. Field Test

Upon conducting a numerical simulation analysis and taking into account the site's actual conditions, three gas drainage drilling fields were established in the 81201 working face of the coal mine. The initial drainage drilling field is situated 55 m from the working face's open-off cut, with subsequent fields spaced 100 m apart. Each field consists of three boreholes, resulting in a total of nine boreholes. The drilling parameters are detailed in Table 6.

Table 6. Drilling field parameters of high directional long drilling.

Numbering	β/°	θ/°	α/°	Bore Length (m)	Borehole Diameter (m)
1	8	15	28	236	115
2	9	17	31	239	115
3	9	18	32	242	115
4	12	16	34	243	115
5	14	19	35	242	115
6	16	21	35	240	115
7	19	23	42	241	115
8	18	20	41	240	115
9	19	23	40	242	115

In Table 6, β is the elevation angle, θ is the azimuth angle, and α is the rotation angle. As perfecting the actual operation of a borehole during on-site drilling is difficult, a certain elevation angle and inclination angle were generated, but the error was still within a certain

range. The calculated error was very small, and the gas extraction rate was only affected by about 2%.

Figure 12 is a schematic diagram of the arrangement of high-level drainage boreholes. The angle, length, and diameter of the No. 1, 2, and 3 boreholes are shown in Table 6.

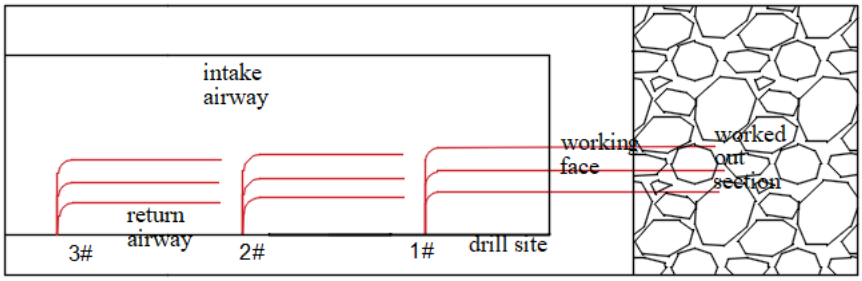


Figure 12. High-level drilling arrangement of the 81201 working face.

The aforementioned scheme was executed at the 81201 working face, where the gas purity flow and concentration were meticulously monitored within the main pipeline of two drilling fields [36]. The monitoring period spanned 100 days, and a curve illustrating the gas purity flow and concentration was generated based on the optimized data, as depicted in Figure 13.

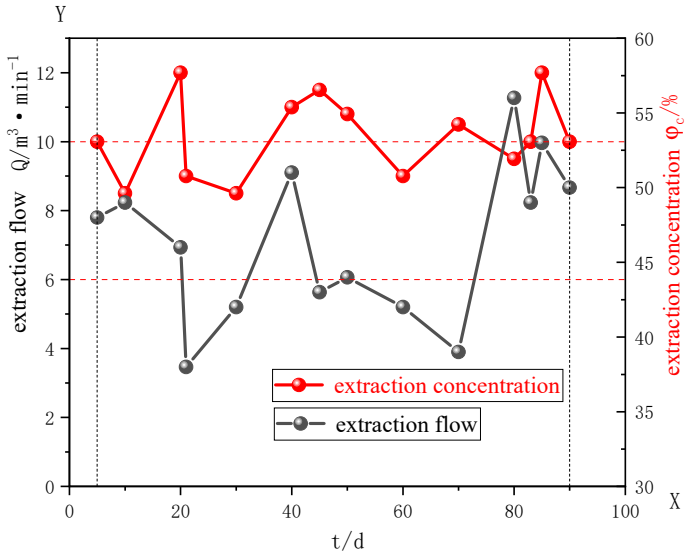


Figure 13. Pure flow rate and gas concentration curves of optimized gas extraction.

As depicted in Figure 13, subsequent to the optimization of drilling protocols, the peak pure gas extraction flow rate within the drilling field was 9.91 m^3/min, with the minimum rate observed at 6.1 m^3/min and the average pure flow rate being around 8 m^3/min. The drilling field's maximum gas concentration reached 57.2%, the minimum stood at 38%, and the average gas concentration was approximately 47.5%. The gas concentrations at the working face, upper corner, and return-air roadway were monitored after drilling optimization, illustrated as a gas concentration variation curve in Figure 14 [37].

As illustrated in Figure 14, the gas concentration in the upper corner of the optimized working face fluctuated from 0.15% to 0.35%. Similarly, the gas concentration within the working face itself fluctuated between 0.18% and 0.40%, while the return airway experienced variations from 0.28% to 0.42%. Notably, all these concentrations are below those recorded prior to optimization, suggesting favorable extraction efficiency [37].

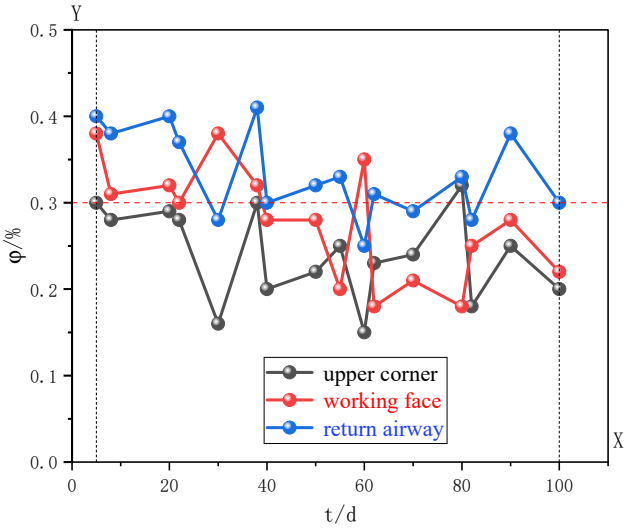


Figure 14. The gas concentration change curve.

6. Conclusions

In this study, the 81201 working face of a coal mine in Shanxi Province was taken as the research object. In view of problems such as the long construction period and high mining cost in traditional high-drainage roadways, the gas extraction principle and advantages of a high-level directional long borehole were analyzed, and the gas extraction horizon, pressure, and borehole trajectory parameters were optimized. The conclusions are as follows:

(1) According to the geological engineering conditions of coal mines, combined with the theory of the mining-induced fracture 'O' ring, the optimal position of the high-level drilling field is determined to be about 23 m above the coal seam and the negative extraction pressure in the 20 kPa drilling field is determined to be 100 m. When the length of the stubble is greater than 35 m and the horizontal distance of the borehole is greater than 37 m, the concentration of the extracted gas is the best. When the drilling angle is 30° and the number of boreholes is set at two, the effect of the gas extraction is better.

(2) The field test revealed that the pure flow rate of the extracted gas increased from its initial 4.0 m^3/min to 8.3 m^3/min following the optimization of the drilling extraction parameters. Additionally, the gas concentration extracted via drilling rose from 17.5% to 46%, while the gas concentration at the upper corner of the working face decreased from 0.91% to 0.33%. Similarly, the gas concentration on the working face itself dropped from 0.86% to 0.29%, and in the return-air roadway, it decreased from 0.82% to 0.23%. These improvements have ensured safe production of the mining face. Furthermore, this study offers valuable insights into the optimization of high-level directional long borehole parameters in other high-gas coal seams.

(3) The goaf gas migration model established during numerical simulation was verified in the experiment. The measured data were quite accurate and good results were achieved, but some errors were also present. For example, the extraction position was set at 23 m, but the actual effect was better at 25 m. The theoretical value for optimal negative extraction pressure is 20 kPa, but the actual extraction pressure was at 23 kPa. Thus, good results, but also greater uncertainties, can be obtained for the corner. Achieving accurate values based on current drilling technology is difficult. The error is about 3^0 in the current technical case, and such operations are difficult. However, a theoretical analysis of this drilling trajectory does have great advantages and is worthy of further study.

(4) According to our field data, compared with the data from references [38] for studies conducted during the same experimental period on the use of the traditional high-level

borehole extraction method to extract the gas content from the same coal mine, we found that the extraction of gas pure flow increased by 2.0 m^3/min, the borehole gas concentration increased by 23%, the working face gas concentration decreased by 0.26%, the return-air roadway gas concentration decreased by 0.5%, and the data indicators improved [39,40].

Author Contributions: Formal analysis, K.G.; Resources, S.M. All authors have read and agreed to the published version of the manuscript.

Funding: This research received no external funding.

Data Availability Statement: No new data were created or analyzed in this study.

Conflicts of Interest: The authors declare no conflict of interest.

References

1. Wang, H.; Wang, E.; Li, Z.; Liu, X.; Liu, X.; Wang, K. Analysis of the Difference of Gas Extraction Quantity from Coal Seam under the Influence of Permeability, Gas Pressure, and Buried Depth of Coal Seam: A Case Study. *Processes* **2023**, *11*, 3086. [CrossRef]
2. Yan, J.; Zhang, M.; Zhang, W.; Kang, Q. Simulation Study on the Characteristics of Gas Extraction from Coal Seams Based on the Superposition Effect and Hole Placement Method. *Sustainability* **2023**, *15*, 8409. [CrossRef]
3. Lin, X.; Liu, Z.; Geng, N.; Hu, P.; Gu, Q. Optimization and Application of Water Injection Process in Gas-Bearing Coal Seam. *Processes* **2023**, *11*, 3003. [CrossRef]
4. Wang, K.; Wang, Y.; Xu, C.; Xu, Z.; Guo, H.; Liu, Y.; Dong, H. Transition of dominated factors in coal seam gas migration: Thermo-hydro-mechanical modeling and analysis. *Int. J. Heat Mass Transf.* **2024**, *236*, 126239. [CrossRef]
5. Lv, X.; Hu, S.; Nian, J.; Deng, C.; Zhao, B.; He, C.; Wang, Y.; Zhang, X.; Zhang, W. Gas migration control in goaf with double roof cutting and retaining roadway. *Sci. Rep.* **2024**, *14*, 29743. [CrossRef]
6. Shen, J. Working face gas control technology based on directional interception borehole. *Shandong Coal Sci. Technol.* **2021**, *39*, 109–111+114.
7. Li, C. Comparative analysis of the effect of U + L and U + I ventilation on gas emission. *J. Shanxi Energy Univ.* **2020**, *33*, 4–6.
8. Li, J.; Guo, P.; Xie, W.; Chu, J.; Yin, Z.; Yuan, A.; Zhang, M.; Jiao, Z. Experimental Study on Adsorption Pore Structure and Gas Migration of Coal Reservoir Using Low-Field Nuclear Magnetic Resonance. *Adv. Civ. Eng.* **2020**, *2020*, 8839819. [CrossRef]
9. Kong, Y. Research on the status quo and development trend of coal mine gas control in China. *Sci. Technol. Wind.* **2020**, 126.
10. Nian, J.; He, C.; Zhao, B.; Lv, X.; Deng, C. Asymmetric development of overburden fracture and gas migration law for a goaf of entry formed by roof cutting. *Energy Sci. Eng.* **2024**, *12*, 4070–4089. [CrossRef]
11. Zhang, F. Buried pipe extraction technology of 1106. *Jiangxi Coal Sci. Technol.* **2020**, 48–51.
12. Li, F.; Luo, H.; Wang, C. Study on the distribution law of the "three belts" of spontaneous combustion under the buried tube extraction in the goaf area. *All Coal Mine* **2020**, *51*, 169–173.
13. Li, M.; Liu, Y. Research on gas extraction technology by vertical drilling hole of thick coal seam mining ground. *Coal Technol.* **2020**, *39*, 100–101.
14. Du, J. Experimental study on gas extraction drilling hole in the bottom of high outburst mine. *Yunnan Chem. Ind.* **2020**, *47*, 155–156+159.
15. Zhang, X.; Chen, F. Research on the desorption law and diffusion kinetic properties of gas in raw coal and tectonic coal. *Fuel* **2024**, *376*, 132653. [CrossRef]
16. Miao, Y.; Zhao, C.; Zhou, G. Gas flow rate evaluation in coal coupling the matrix shrinkage effect caused by water extraction. *J. Energy Resour. Technol.* **2022**, *144*, 032301. [CrossRef]
17. Cheng, X.; Cheng, C.; Xiao, L.; Ma, X. Response Surface Analysis on Multiple Parameter Effects on Borehole Gas Extraction Efficiency. *Processes* **2024**, *12*, 1587. [CrossRef]
18. Zhang, T.; Li, J.; Ji, X.; Ji, B.; Feng, G.; Pan, H.; Pang, M. Coherence analysis of the crack strain field in coal rock with borehole-crack composite defects. *Theor. Appl. Fract. Mech.* **2024**, *133*, 104497. [CrossRef]
19. Gao, H.; Du, F.; Cheng, X.; Zhang, J.; Zhou, A. Study on the Influence Mechanism of Air Leakage on Gas Extraction Effect—A Numerical Case Study of the Coal Mine Site in Anhui. *Processes* **2023**, *11*, 2161. [CrossRef]
20. Zhang, T.; Ji, X.; Pang, M.; Zhang, L.; Ji, B.; Yang, W.; Pan, H. Investigation of the crack evolution characteristics of coal and rock bodies around boreholes during progressive damage based on stress threshold values. *Theor. Appl. Fract. Mech.* **2023**, *125*, 103935. [CrossRef]
21. Du, Z.; Chen, D.; Li, X.; Jian, Y.; Zhang, W.; Zhang, D.; Tian, Y. Study on the Partial Paste Backfill Mining Method in a Fully Mechanized Top-Coal Caving Face: Case Study from a Coal Mine, China. *Sustainability* **2024**, *16*, 4393. [CrossRef]

22. Fu, J.H.; Chen, D.Y.; Li, X.; Li, H.; Liu, S.; Li, C.; Zhang, J.W. Research on the technology of gob-side entry retaining by pouring support beside the roadway in "three soft" coal seam: A case study. *Phys. Fluids* **2024**, *36*, 017123. [CrossRef]
23. Zhang, D.; Zhang, M.; Zhang, S.; Wang, Z.; Jin, Y.; Liu, R. Numerical Simulation of Effective Extraction Radius of Pre-Drainage Borehole Based on Coal Damage Model. *Sustainability* **2023**, *15*, 4446. [CrossRef]
24. Wu, Y. Coal mine gas prevention and control has produced excellent results. *China Energy News*, 15 March 2021.
25. Yang, S.; Han, Q. Accurate control range determination and effect analysis of high drilling extraction in the island working face. *Energy Technol. Manag.* **2021**, *46*, 38–39.
26. Lee, V. Application of high directional long drilling extraction technology in gas control in upper corner. *Mod. Coal Mine* **2021**, *30*, 91–94.
27. Zhang, F.; Wang, H. Optimization of Drilling Parameters in Influence Area of Gas–Solid Interaction during Parallel Drilling Hole. *Processes* **2023**, *11*, 2371. [CrossRef]
28. Li, W.; Yang, K.; Deng, D.; Zhao, C.; Yang, S.; Cheng, Y.; Lu, S. A lattice Boltzmann model for simulating gas transport in coal nanopores considering surface adsorption and diffusion effects. *Fuel* **2023**, *340*, 127507. [CrossRef]
29. Lan, T.; Zhang, Z.; Le, Q.; Liu, Y.; Wang, S. Study on the influence of the tectonic evolution of Shuangyashan Basin on gas occurrence and extraction in mines. *Front. Earth Sci.* **2023**, *10*, 1083489. [CrossRef]
30. Niu, Y.; Song, X.; Li, Z.; Wang, E.; Liu, Q.; Zhang, X.; Cai, G.; Zhang, Q. Experimental study and field verification of stability monitoring of gas drainage borehole in mining coal seam. *J. Pet. Sci. Eng.* **2020**, *189*, 106985. [CrossRef]
31. Zuo, S.; Wang, C.; Liao, Y.; Peng, S.; Ma, Z.; Zhang, L. Mechanism of a novel ultrasonic promoting fracturing technology in stimulating permeability and gas extraction. *Energy Rep.* **2022**, *8*, 12776–12786. [CrossRef]
32. Zhang, L.; Wu, W.; Bian, Y.; Yang, M.; Luo, H. Influences of Gas Drainage Pipe Positions on Spontaneous Coal Combustion in the Gob: A Case Study of Baode Coal Mine in China. *Combust. Sci. Technol.* **2022**, *194*, 3357–3373. [CrossRef]
33. Guo, J.; Wang, L.; Ding, K.; Jiang, C.; Wang, S.; Ren, B. A Preliminary Experimental Study on the Effect of Confining Pressure or Gas Pressure on the Permeability of Coal Samples. *Minerals* **2022**, *12*, 1265. [CrossRef]
34. Li, Y.; Dong, H.; Guo, X. Research on the Determination Technology of Key Position of Sealing Holes for Gas Extraction Drilling in Zhangcun Coal Mine. *Adv. Civ. Eng.* **2022**, *2022*, 10663836. [CrossRef]
35. Yang, L. Research on Reasonable Hole Arrangement Parameters of Ground Drilling Gas Extraction Technology; Research on Reasonable Hole Arrangement Parameters of Ground Drilling Gas Extraction Technology. *J. Appl. Sci. Eng. Innov.* **2020**, *7*, 103–105.
36. Qin, M. Applied Research on Gas Extraction Technology in High Output and High Efficiency Mine Goaf; Applied Research on Gas Extraction Technology in High Output and High Efficiency Mine Goaf. *J. Appl. Sci. Eng. Innov.* **2020**, *7*, 59–62.
37. Yang, L. Research on Complete Set of Gas Drainage Technology for Coal Mine Long Bedding Drilling. *J. Appl. Sci. Eng. Innov.* **2020**, *7*, 73–77.
38. Qian, Z. Research on Multi-directional Gas Drainage Technology in Goaf of Working Face. *IOP Conf. Ser. Earth Environ. Sci.* **2020**, *526*, 012167. [CrossRef]
39. Xu, C.; Wang, K.; Li, X.; Yuan, L.; Zhao, C.; Guo, H. Collaborative gas drainage technology of high and low level roadways in highly-gassy coal seam mining. *Fuel* **2022**, *323*, 124325. [CrossRef]
40. Shuang, H.; Meng, W.; Zhai, Y.; Xiao, P.; Shi, Y.; Tian, Y. Application and Optimization of the Parameters of the High-Level Boreholes in Lateral High Drainage Roadway. *Sustainability* **2022**, *14*, 16908. [CrossRef]

Disclaimer/Publisher's Note: The statements, opinions and data contained in all publications are solely those of the individual author(s) and contributor(s) and not of MDPI and/or the editor(s). MDPI and/or the editor(s) disclaim responsibility for any injury to people or property resulting from any ideas, methods, instructions or products referred to in the content.